Polarization and intensity spectra for Mg-Ne and Mg-Ar fractional collisions

D. A. Olsgaard,* R. A. Lasell, M. D. Havey, and A. Sieradzan†
Physics Department, Old Dominion University, Norfolk, Virginia 23529
(Received 5 April 1993)

Extensive experimental studies of Mg-Ne and Mg-Ar fractional collisions are reported. In the fractional-collision process, two-color, two-photon absorption takes place during a single binary collision. Polarization and relative intensity spectra were measured in an approximately $\pm 50\text{-cm}^{-1}$ range around the atomic Mg $3s\ ^1S_0 \rightarrow 3p\ ^1P_1 \rightarrow 5s\ ^1S_0$ two-photon resonance. The generally-weak-field spectra show a remarkable phenomenology associated with the relative linear-polarization directions of the two exciting laser beams and with their separate detunings from atomic one-photon resonance. The polarization and relative absorption spectra display effects due to relative detuning, multiple Condon points, and laser intensity. Details of our experimental approach, and spectra for the process in Mg-Ar and Mg-Ne are presented and discussed. The data are seen to contain information on the short-range collision dynamics of the Mg–rare-gas pairs, and on the development of the alignment over the course of the collision.

PACS number(s): 33.80.Gj, 34.80.Qb, 33.80.Wz

I. INTRODUCTION

Experimental study of atomic collisions continues to undergo remarkable evolution in the detail of collision processes determinable by direct measurement. Experiments in an atomic beam regularly select the initial internal atomic states, and determine the final ones as a function of the scattering angles and the scattering energy [1]. These experiments can be complete in the sense that all measurable quantities associated with the full collision may be found by experiment. However, it is possible to determine additional information about the collision dynamics by probing the colliding pair during the collision process itself. This may be accomplished in the time domain by direct resolution of polarization or population dynamics on a femtosecond time scale [2], or in the frequency domain by nonresonant excitation of the colliding pair [3–5] with moderately narrow-band light sources. In the sense that the angular and energy dependence is not directly measured, the frequency-domain studies have yet to reach the sophistication of the atomic-beam measurements. Even at the current level of development, however, so-called optical collision experiments provide experimental information not accessible in other ways. For example, excitation within specific ranges of detunings from resonant pumping of the atomic participants can correspond to selection of specific molecular states involved in the collision process. Then the degree to which those states are important to either inelastic or depolarization processes may be assessed. Dynamical correlation of electronic and kinetic degrees of freedom are particularly evident in the results of this type of experiment. Recently, selection of the angular momentum (in photodissociation [6]) or alignment (in optical collisions [7]) of the initial states has been accomplished.

We have presented a preliminary report [8] of an extension of the optical collision method whereby two photons are absorbed in a single collision [9–11]. In this approach, a molecular alignment [12] is produced by absorption of nonresonant polarized light. The alignment is then probed, also within the molecular regime, by further absorption of polarized light from a second nonresonant light source. As the alignment dynamics are determined over only a portion of the collision trajectory, the collisions are termed fractional collisions. In this report, considerable elaboration of our experimental technique is made, and extensive results are presented and discussed for fractional collisions between Mg and Ne or Ar atoms.

II. OVERVIEW OF PHYSICAL PROCESSES

It is useful to consider atomic collisions in terms of the time scale τ associated with the various physical processes. For optical collisions this is normally a subpicosecond time interval associated with the dynamics in the molecular regime. At considerably longer intervals, inverse predissociation (or alternately, scattering resonances) may be important. For bound state spectroscopy of molecular electronic states, a radiative or collisional lifetime of nanoseconds or longer is the determinant of the width of Doppler-free rovibrational transitions. The various spectroscopies then form a continuum of possibilities within which interactions having an associated frequency ω become important as $\omega\tau \rightarrow 1$. As will be seen in the results section of this paper, a single fractional-collision absorption or polarization spectrum may consist of regions dominated alternatively by either free scattering processes or by bound-bound electronic transitions. Although the bound state spectra contain important information on the dynamics and on the states involved in the collision, we will be concerned here primarily with the free-free scattering portion of the molecular alignment spectrum.

The overall process may be visualized with the aid of Fig. 1, which shows qualitative interatomic potentials for the relevant Mg–rare-gas molecular states [13–15]. The

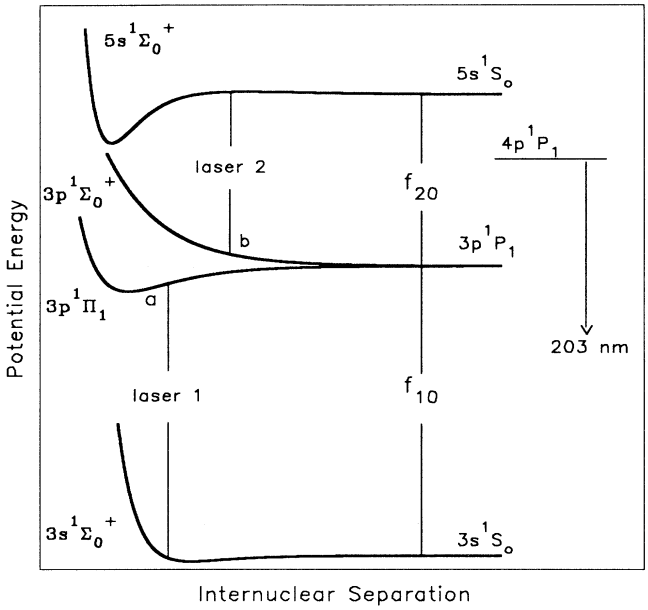

FIG. 1. Schematic potentials and transitions for Mg–rare-gas fractional collisions.

atomic Mg transitions of interest are the $3s\ ^1S_0 \rightarrow 3p\ ^1P_1$ resonance transition at 285.2 nm and the $3p\ ^1P_1 \rightarrow 5s\ ^1S_0$ transition at 571.2 nm [16]. The frequency of each transition is labeled as f_{10} or f_{20}, respectively. According to the classical Franck-Condon principle, molecular radiative transitions take place at internuclear separations (R) where the energy difference between the molecular states is made up by light of energy hf_1 and hf_2. These points are indicated by solid vertical lines in the figure. Detunings from atomic resonance are defined as $\Delta_1 = hf_1 - hf_{10}$ for the $3s\ ^1S_0 \rightarrow 3p\ ^1P_1$ transition and as $\Delta_2 = hf_2 - hf_{20}$ for the $3p\ ^1P_1 \rightarrow 5s\ ^1S_0$ transition. All detunings are given in vacuum cm^{-1} units.

In the absence of collisions, radiative transitions to the atomic Mg $5s\ ^1S_0$ level occur only when $\Delta_1 + \Delta_2 = 0$, corresponding to two-color, two-photon excitation of that level. In the absence of a hyperfine interaction in the $3p\ ^1P_1$ level, the linear polarization degree of these resonances is 100% within the range of detunings accessed in the experiments reported here. Hyperfine [17] depolarization, which occurs in isotopes with nonzero nuclear spin I, will only be significant when Δ_1 and Δ_2 are both nearly zero, corresponding to stepwise excitation of the $5s\ ^1S_0$ level through the $3p\ ^1P_1$ resonance level. Atomic Mg of natural isotopic abundance has three stable isotopes, ^{24}Mg with $I=0$ and a relative abundance of 0.79, ^{25}Mg with $I=\frac{5}{2}$ and a relative abundance of 0.1, and ^{26}Mg, which has $I=0$ and a relative abundance of 0.11 [16]. Although we were unable to locate values of the hyperfine coupling constants in the $3p\ ^1P_1$ level for ^{25}Mg, the hyperfine splitting in this isotope must be such that $\omega_{\rm hf}\tau_1 \ll 1$, where τ_1 is the 2.1-ns radiative lifetime of the resonance level [16].

When collisions are considered, additional excitation of the $3p\ ^1P_1$ and $5s\ ^1S_0$ levels occurs as a result of molecular radiative transitions at the Condon points a and b indicated in Fig. 1. Excitation with laser 1 produces Mg dissociation products having a distribution of average multipoles $\langle T_q^k \rangle$ [12], having rank k and component q, within the $3p\ ^1P_1$ level. For excitation with linearly polarized light in an isotropic collision environment, which is the case considered in this paper, only population $\langle T_0^0(\Delta_1) \rangle$ and alignment $\langle T_0^2(\Delta_1) \rangle = \langle A_0(\Delta_1) \rangle$ will be produced. As indicated, these quantities will depend on the detuning of laser 1 from resonant excitation (when $\Delta_1 = 0$). As has been shown by many experiments and calculations, both the population and the alignment in the resonance level depend significantly on variations in the species involved in the collision and on the detuning Δ_1. In terms of the scheme indicated in Fig. 1, probing these multipoles is achieved by adjusting laser 2 so that $\Delta_2 = 0$.

When Δ_2 is tuned away from the $3p\ ^1P_1 \rightarrow 5s\ ^1S_0$ resonance, the population and alignment [3] within the molecule itself is probed. For the particular situation shown in Fig. 1, laser 1 produces initial multipoles via pumping at the Condon point a, corresponding to excitation of the $3p\ ^1\Sigma_0^+$ molecular electronic state. Following evolution within the molecular frame, these are probed at a larger internuclear separation, by laser 2, at the Condon point indicated by b. Variation of Δ_2 for each value of Δ_1 then maps out the dynamical evolution of the measured quantities over a range of internuclear separations R. Systematic variation of the two detunings generates a surface for each multipole which contains information on the dynamics of that multipole within the intermediate states. For the cases considered here, intensity and polarization surfaces have been generated, these being equivalent to population and alignment surfaces.

In addition to the stepwise molecular process just described, direct two-photon molecular transitions between the $3s\ ^1\Sigma_0^+$ and the $5s\ ^1\Sigma_0^+$ electronic states are possible. Within the framework of the classical Franck-Condon principle, these transitions occur when the sum of the detunings $\Delta_1 + \Delta_2$ is made up by the difference in the potentials of the two states. The strength and polarization of direct transitions depend on the distribution of contributing intermediate states. These are mainly the bound and continuum levels associated with the $3p\ ^1\Sigma_0^+$ and the $3p\ ^1\pi^{\pm}$ Mg–rare-gas electronic states. The polarization of the direct transitions should not depend directly on the dynamics within the intermediate states, but instead on the electronic symmetry of the states involved and the amount of nonadiabatic mixing within them.

For both direct and stepwise excitation processes, bound levels associated with any of the electronic states involved may be important to the spectra. For example, laser 1 may excite bound levels within the $3p\ ^1\pi^{\pm}$ electronic state, either through bound-bound molecular transitions or through a free-bound capture process. These, in turn, can be probed by laser 2, leading to excitation of either bound or dissociative levels within the $5s\ ^1\Sigma_0^+$ state. The polarization of bound intermediate levels should depend sensitively on the amount of Λ doubling [18] within them and on the radiative or collisionally lim-

ited lifetime of the levels. As will be discussed in the results section of this paper, regions of the spectrum associated with bound-bound transitions are readily identified by saturation of the excitation spectra [19]. Laser intensities were insufficient to saturate the free-free portions of the excitation spectra. It should also be pointed out that, as the results of this paper were obtained from gas cell experiments, the polarization and intensity results represent averages over several variables, including impact parameter, angular momenta of the colliding pair, and a thermal distribution of collision energies. Nevertheless, the variations of the spectra with detuning, polarization, collision partner, and laser power provide a rich phenomenology associated with the two-photon, fractional-collision process.

Finally, we briefly discuss some qualitative aspects of the fractional-collision process that can be visualized by considering the collision partners to move on classical trajectories, and by assuming that radiative transitions take place in the vicinity of localized Condon points. First note that for collisions with some maximum impact parameter R, the maximum contributing angular momentum for the process $l_{\max}$ is given semiclassically by $\mu v R/\hbar$, where $\hbar$ is Planck's constant divided by 2π, μ is the reduced mass of the colliding pair, and v the asymptotic magnitude of the relative velocity of the Mg and rare-gas atoms [20]. So long as the collision energy is large enough compared to the internuclear potentials that the collision trajectories are straight lines, R may be approximated as the Condon point for an optical collision. This permits an estimate of $l_{\max}$. For stepwise excitation, $l_{\max}$ is determined in the first step of the radiative process. The maximum angular momentum is about $70\hbar$ for Mg-Ar, and is considerably smaller than the range of angular momenta contributing to full collision processes. Second, depending on the relative detunings of laser 1 and laser 2, either incoming or both incoming and outgoing trajectories in the intermediate states can contribute to the amplitude brought to the final $5s\ ^1\Sigma_0^+$ molecular state. For example, in the situation illustrated in Fig. 1, both incoming and outgoing trajectories in the intermediate $3p\ ^1\Sigma_0^+$ state contribute amplitude to the probe transitions at Condon point b. On the other hand, if laser 2 were tuned so that probe transitions would occur at smaller internuclear separations than the Condon point R_a, then only initially incoming trajectories in the intermediate state would contribute to the final state amplitude.

III. EXPERIMENTAL DETAILS

A block diagram of the experimental apparatus is shown in Fig. 2. There two pulsed dye lasers are pumped by a few percent of the 120-mJ green output of a neodymium yttrium aluminum garnet (Nd:YAG) laser. The dye lasers are each of a grazing incidence design, and have an output of about 200 μJ in a 6-ns pulse width. The bandwidth of each laser is less than 3 GHz. The output of

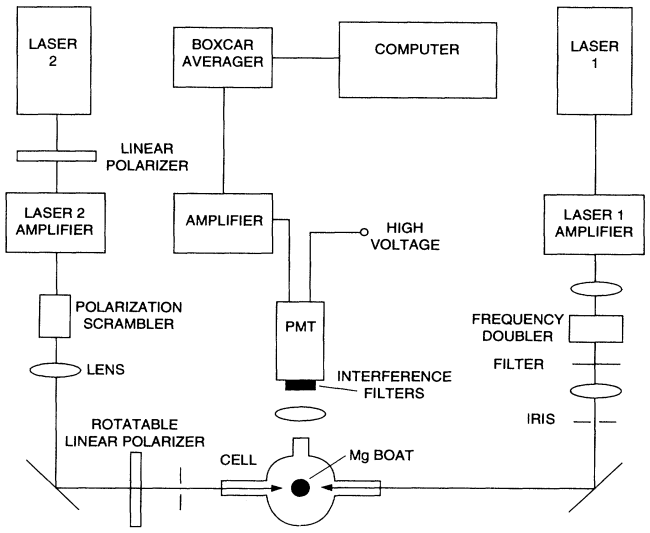

FIG. 2. Block diagram of the experimental apparatus. PMT denotes a photomultiplier tube.

each laser is further amplified by about a factor of 10 in a single stage of amplification. The output of laser 1 is then frequency doubled by focusing its output into an angle-tuned potassium dihydrogen phosphate (KDP) crystal, producing radiation in the vicinity of the atomic Mg $3s\ ^1S_0 \rightarrow 3p\ ^1P_1$ transition at 285.2 nm. A 1-mm-thick Schott UG-11 colored-glass filter is used to remove the fundamental dye-laser radiation. It transmits less than 10^{-4} of the fundamental radiation, while passing more than 85% of the desired ultraviolet light. Pulse energies are typically about 20 μJ in a pulse width $\sim$3 ns. The output of laser 1 is strongly linearly polarized in a horizontal plane. The amplified laser 2 beam has a wavelength around 571.2 nm and consists of approximately 1-mJ pulses having a temporal width of about 6 ns. The laser 2 beam is expanded to a diameter of about 1 cm and then passed through a Babinet-Soleil compensator [21] adjusted to scramble the polarization across the beam cross section. Passage of the (laser 2) beam through a rotatable linear polarizer then allows variation of the angle θ between the linear polarization directions of the two laser beams. In separate measurements, the intensity of laser 2 was found to vary by less than 2% as the angle θ was varied over its full range of $0-2\pi$. The two beams are then weakly focused and then made to pass collinearly, but in opposite directions, through a sample cell. Each beam has a cross section of about 4 mm in the interaction region of the cell.

The sample cell consists of a 250-cm^3 Pyrex sphere on which are mounted four side arms in a horizontal plane at 90° from each other. The two laser ports have a diameter of 2.5 cm and a length of 5.5 cm from the surface of the cell. Quartz windows are attached to the ports with high vacuum epoxy. The other two ports are used for viewing the interaction region of the cell; each has a diameter of 3.8 cm and a length of 4.5 cm. One port is mounted with a uv-grade window, while the other is

sealed by a boro-silicate glass window. Magnesium vapor is generated in the cell by heating a stainless steel boat located just below (~ 1 cm) the interaction region of the cell. The boat is mounted on a quartz tube, which in turn is supported by a conflat flange located on a fifth port extending 9 cm below the base of the spherical cell. The boat is a cylindrical oven of about 3 cm length and 0.5 cm diameter; the wall thickness is about 0.5 mm. It is heated by an 80-W internal coaxial heater wound inside the oven. The approximate boat temperature is monitored by a Chromel-Alumel thermocouple attached to the outside of the boat. A commercial oven controller provides both heater power and feedback from the thermocouple output, resulting in a temperature stability of ± 0.2 K at the normal oven operating temperature of 590 K. Magnesium metal chips are packed in the oven; the equilibrium vapor density in the boat under the usual operating conditions is about 10^{12} cm^{-3}. This results in an estimated density of roughly 10^{11} cm^{-3} in the interaction region of the cell. The entire sample cell arrangement is attached to an oil-free, vacuum-gas handling system allowing for evacuation of the cell to less than 10^{-6} Torr and for admission of 0–100 Torr research grade rare gas into the cell. The rare-gas pressure is determined by a capacitance manometer having a rated accuracy of 0.1 Torr.

Population produced in the Mg $5s\ ^1S_0$ level is monitored through the $4p\ ^1P_1 \rightarrow 3s\ ^1S_0$ cascade fluorescence at 202.6 nm. The fluorescence is collected at 90° from the laser beams and concentrated on the cathode of an EMI 9814 photomultiplier tube (PMT) by a 7.5-cm focal length quartz lens. The radio-frequency-shielded PMT has a bialkali cathode and a quartz window to permit detection of ultraviolet light. In order to eliminate the intense scattered laser light and other atomic emission from the cell, the PMT was mounted with well-blocked interference filters which passed about 2% of the desired fluorescence light. Other than the desired cascade fluorescence, the predominant emission from the cell is the intense $3p\ ^1P_1 \rightarrow 3s\ ^1S_0$ resonance fluorescence at 285.2 nm; the filter stack passed a residue of this light amounting to less than 10% of the weakest two-photon fractional-collision signals reported here. As described in a following paragraph, this residue was subtracted from the raw data prior to generating intensity or polarization spectra.

The PMT output was amplified and integrated over a 20-ns interval in order to broaden the single-photon pulses typical of the weaker signals. That portion of the output within a 350-ns gate opened about 40 ns after the laser pulses ended was further integrated by a boxcar averager operated in a last sample mode. The boxcar output level was then digitized by a 12-bit analog-to-digital converter. Signals were accumulated for further analysis in a laboratory computer. For each polarization measurement, four sets of data were obtained. These sets determined the average baseline for each run, the average background due to the resonance radiation leakage through the filters, an average raw signal with the polarization of the two lasers parallel, and an average raw signal with the polarization of laser 2 set perpendicular to that of laser 1. Normally 1000 laser shots were used to accumulate the average signal levels, while 250 laser shots were used to determine the baseline and background levels. Subtraction of baseline and background levels from the signal channels yielded the basic quantities $I_\parallel$ and $I_\perp$ determined by the measurements. From these, detuning-dependent polarization P_L and intensity spectra I_0 were formed according to $P_L = (I_\parallel - I_\perp)/(I_\parallel + I_\perp)$ and $I_0 = I_\parallel + 2I_\perp$. Each polarization measurement reported in this paper represents the average of two to eight individual such runs. At each set of detunings, an intensity measurement was taken at an angle of 54.7°. Normally one or two runs were taken, each run giving two measurements of I.

When detuning-dependent excitation spectra were obtained, the relative linear polarization directions of laser 1 and laser 2 were set at an angle of 54.7° [12] for which the measurements are independent of the alignment of the colliding system. At each Δ_1, a reference detuning Δ_2 was chosen where the intensity spectrum was not rapidly varying with detuning. Frequent measurement of the signal at this detuning after measurement of the intensity at other detunings allowed for normalization of the spectra to variations in Mg density, average laser power, and experimental quantities such as optical alignment and electronic gain drifts.

The data obtained reflect the average cylindrical symmetry induced by the linearly polarized light from laser 1 in the collision frame. Although each collision has a well-defined collision plane, this is not selected directly here; thus the average collision environment is isotropic, and the measurements then have an axial symmetry about the laser 1 polarization direction. Under these circumstances, the physical situation may be described in terms of population (rank 0) and alignment (rank 2) multipoles. These quantities are measured by I_0 and P_L, respectively. For an axially symmetric system, the intensity of the signal induced by laser 2 has the form $I(\chi) = I_0\{1 + (h^{(2)}/4)\langle A_0 \rangle [1 + 3\cos(2\chi)]\}$, where I_0 is a constant measuring the overall strength of the process normalized by the detection efficiency of the apparatus, $h^{(2)}$ is a geometric quantity determined by the angular momenta of the participating states, and $\langle A_0 \rangle$ is the average alignment in the intermediate levels [12]. The angle χ is the angle between the linear polarization directions of laser 1 and laser 2. Thus $I(\chi = 0) = I_\parallel$, while $I(\chi = \pi/2) = I_\perp$. The experiment then determines the quantities I_0 and $h^{(2)}\langle A_0 \rangle$, which generally depend on both Δ_1 and Δ_2. The quantity I_0 depends on the strength of the two-photon fractional-collision process, but also on the overall experimental detection efficiency, both laser intensities, and the Mg density. These experimental quantities are not sufficiently well determined in the experiments to obtain meaningful absolute intensity spectra. Instead, we report relative excitation spectra for which the various experimental quantities are held constant. Further, even though the alignment-dependent quantity $h^{(2)}\langle A_0 \rangle$ may readily be obtained, the linear polarization degree P_L is most directly related to the measurements. Thus our results are presented in terms of I_0 and P_L.

IV. RESULTS AND DISCUSSION

A. General observations

All results presented in this paper are free of measurable systematic effects associated with variations in the Mg density, background due to dye-laser fluorescence and interference filter leakage, and due to operation of the polarimeter. Increasing the signal size about a factor of 10, by increasing the Mg density, led to no measurable change in P_L within an uncertainty of about 2%. Background levels due to dye-laser amplified spontaneous emission (ASE) were kept at a level less than 1% of the total signal size by taking special care with laser alignment and dye concentration. This background appears in optical collision experiments via resonant excitation of the Mg atoms by that portion of the ASE overlapping the atomic Mg absorption lines; signals from this process can be competitive in size with those from the optical collision process. Finally, as discussed in the preceding section, the polarimeter, consisting of a Babinet-Soleil compensator and a rotatable linear polaroid, had associated systematic errors of less than 2%.

Systematic effects due to both rare-gas pressure variations and changes in the laser intensities were observed. The first of these was not important for the nonresonant polarization measurements, while the second had a strong effect on the signal line shape and a lesser influence on P_L. Measurements of P_L with nonzero Δ_1 and Δ_2 were insensitive to variations in the intensity of either laser 1 or laser 2. For resonant excitation or probing of the $3p\ ^1P_1$ level a weak intensity dependence of P_L was observed only when one or both of the transitions was strongly saturated. This behavior has been reported and explained for pump-probe linear polarization experiments in Ca by Belsley *et al.* [22]. The detailed dependence of the results on these quantities will be discussed in the following subsections.

B. Excitation spectra

Measurements of the excitation profile I_0 as a function of Δ_1 and Δ_2 were insensitive to laser power in studies of the Mg-Ne system. In contrast, for $\Delta_1<0$ and $\Delta_2<0$ in the Mg-Ar system, strong saturation of the excitation profile was observed. As shown in Fig. 3, a strong enhancement of the intensity profile is seen over a 30-cm^{-1} range centered near $\Delta_2=-40\ cm^{-1}$. In fact, the enhancement is much stronger than indicated there, for the signal in the central part of this region is strongly saturated to variations in the laser 2 intensity. Outside this region the signals varied approximately linearly with the intensity of laser 2. The signal size in both cases was linear with the intensity of laser 1. A possible explanation for this behavior is that laser 1 excites bound levels within the Mg-Ar $3p\ ^1\pi_1$ potential, and that these are probed by laser 2 on bound-bound transitions to the $5s\ ^1\Sigma_0^+$ electronic state. The intensity of laser 2 is easily sufficient to saturate bound-bound transitions, but should not be large enough to saturate free-bound or free-free transitions. Spectroscopic data [13] for the $3s\ ^1\Sigma_0^+$ and

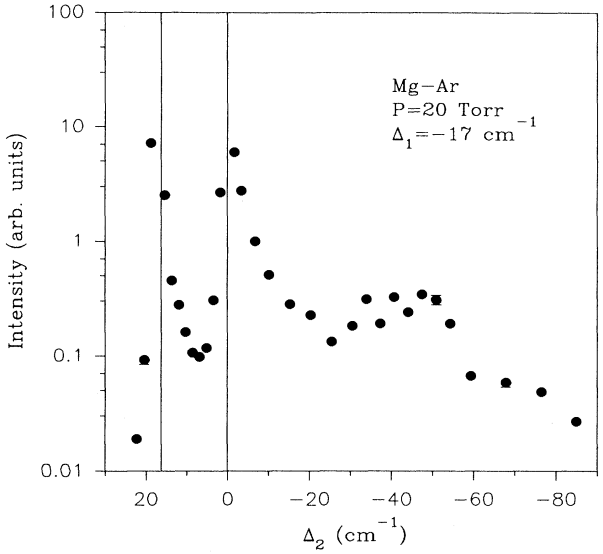

FIG. 3. Relative Mg-Ar fractional-collision excitation spectrum for $\Delta_1=-17\ cm^{-1}$.

the $3p\ ^1\pi_1$ states of Mg-Ar show that $\Delta_1<0$ corresponds to excitation into the bound portions of the intermediate π state. Further, calculations of potentials [15] for excited $ns\ ^1\Sigma^+$ potentials in Mg-Ar indicate that they should be bound by several hundred cm^{-1}, and thus support bound rotational-vibrational levels in the spectral region probed by laser 2. On the other hand, a recent experiment on Mg-Ne shows only very weak binding in the $3p\ ^1\pi_1$ state, consistent with the relative binding in alkali-metal–Ne versus alkali-metal–Ar molecules [23]. As the $3p\ ^1\pi_1$ potential should support few bound levels, saturation effects should not be seen in this region for Mg-Ne. Thus this region of the spectrum is an important one for high-resolution studies of the rovibrational spectra of electronically excited states in Mg-Ar, but does not contain clean information about the dynamics of the fractional-collision process.

The excitation spectra were taken at a rare-gas pressure of $P=20$ Torr, where the signals were large enough to obtain reliable shapes over a wide range of detunings. The size of the signals at each set of detunings was approximately linear with the rare-gas pressure, although variations in Mg density associated with changes in the pressure prevented quantitative conclusions on this point. When $|\Delta_2|$ is greater than about 10 cm^{-1} in Mg-Ne and greater than around 20 cm^{-1} in Mg-Ar, it is estimated that the subsequent collision contribution to the spectra is no more than about 25%. Thus within the statistical error bars given, the excitation spectra presented here represent nearly the $P\rightarrow 0$ spectra.

Unsaturated relative excitation spectra recorded at several detunings Δ_1 for Mg-Ar and Mg-Ne fractional collisions are presented in Figs. 4 and 5. The spectra are dominated by the atomic Mg two-photon resonance at $\Delta_1+\Delta_2=0$ and by the one-photon optical collision signal occurring when $\Delta_2=0$. Also evident are extended wings,

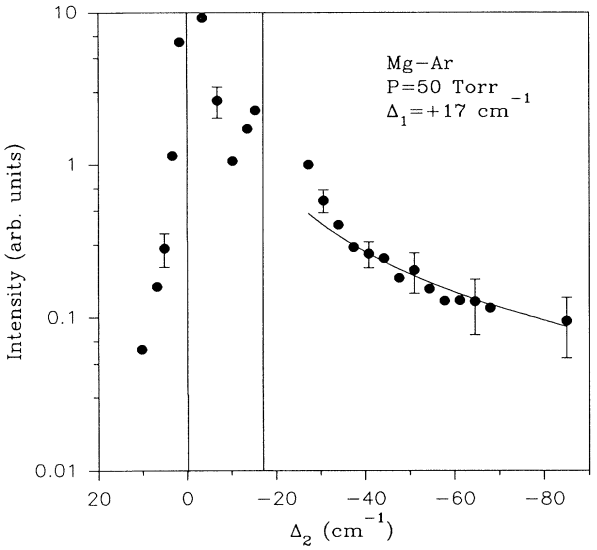

FIG. 4. Relative Mg-Ar fractional-collision excitation spectrum for $\Delta_1 = +17\ \mathrm{cm}^{-1}$.

occurring on either side of these resonances, having pronounced intensity asymmetries depending on the size and sign of the detunings. These are attributed to the two-photon fractional-collision process. The spectra are also strongly asymmetric with respect to the sign of Δ_1, with an extended wing occurring in Mg-Ne for $\Delta_2 < 0$ when $\Delta_1 = -25.5\ \mathrm{cm}^{-1}$. Such a wing also occurs in Mg-Ar for $\Delta_2 < 0$ when $\Delta_1 = 17\ \mathrm{cm}^{-1}$. The qualitative features of the data are quite similar to model spectra for this process calculated earlier by Yeh and Berman [10]. In those calculations, approximate analytical line shapes in selected spectral regions were determined for van der Waals potentials. For Δ_1 within the impact region and Δ_2 in the quasistatic region, the calculations indicate a $1/|\Delta_2|^{3/2}$ dependence of the excitation spectrum on Δ_2. This form is indicated by the solid line in Figs. 4 and 5(b), where the overall vertical scale has been normalized to the intensity at one detuning in each case. Although Δ_1 is outside the impact region, the line shape does appear to have approximately this functional form. Note that, for Mg-Ar in particular, subsequent collisions and the presence of the two-photon atomic resonance lead to an evident departure from this line shape when $\Delta_2 < -30\ \mathrm{cm}^{-1}$. More quantitative comparisons will of course require calculations for the specific cases, and must generally account for the electronically nondegenerate intermediate molecular states, and the detailed shapes of the interatomic potentials for the Mg–rare-gas molecular states.

C. Polarization spectra

First consider the rare-gas (RG) pressure dependence of P_L, which has its origin in collisions subsequent to the two-photon optical collision. As discussed earlier, absorption of light from laser 1 leads to atomic Mg products in the $3p\ ^1P_1$ level. Subsequent collisions with rare-gas atoms produce molecular population which contributes to the total signal derived from the probe laser 2. As the polarization initially produced in the $3p\ ^1P_1$ level is not large, and is further decreased in the subsequent collision, there results a weakly polarized background to the fractional-collision signal. In a first approximation, the total signal depends on rare-gas pressure P according to $I = I_f P + I_s P^2$, where I_f is the fractional-collision contribution to the signal and where I_s is the subsequent collision part of the total measured intensity. Computing a polarization $P_L = (I_\parallel - I_\perp)/(I_\parallel + I_\perp)$ for an unpolarized background gives an inverse polarization P_L^{-1}

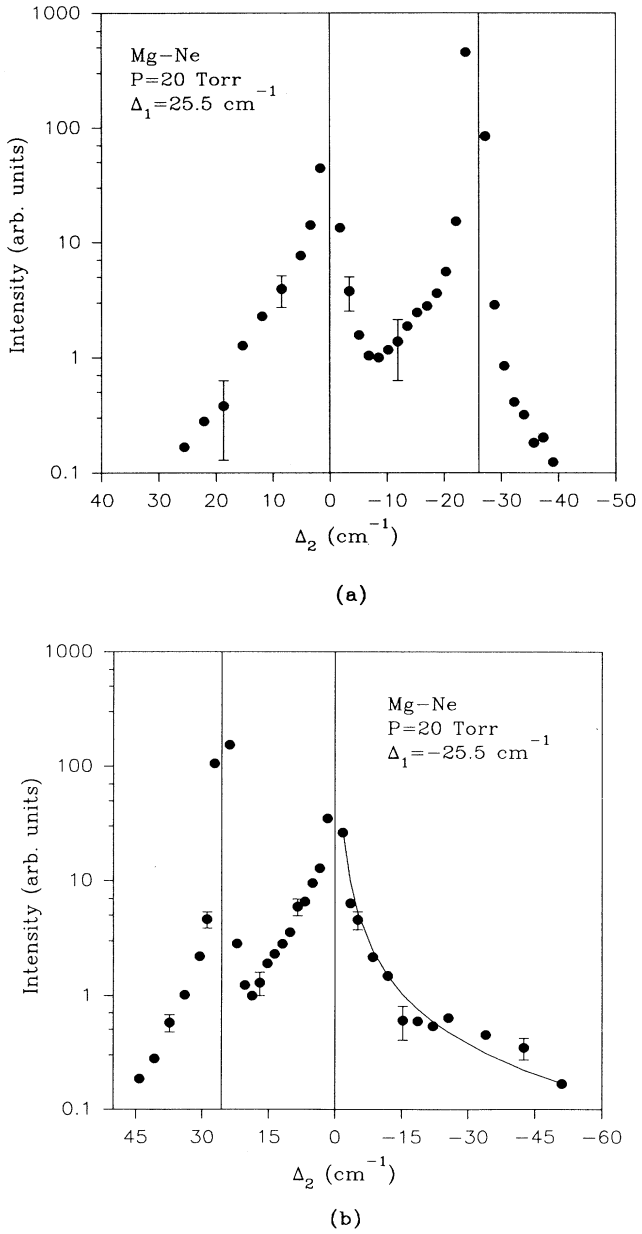

FIG. 5. Relative Mg-Ne fractional-collision excitation spectra: (a) $\Delta_1 = 25.5\ \mathrm{cm}^{-1}$, (b) $\Delta_1 = -25.5\ \mathrm{cm}^{-1}$.

$=P_{L0}^{-1}+mP$, where m is a constant and where P_{L0} is the linear polarization due to the fractional collision only. The slope m may be used to estimate the fraction of the total signal contributed by the subsequent collisions to be less than 25% of the fractional-collision signal. As illustrated in Fig. 6 for Mg-Ne, the Mg-RG fractional-collision polarization data are well described by the expression above. Note that both m and P_{L0} are detuning dependent, and that accurate polarization measurements as a function of pressure are thus required at each detuning in order to extract the physically interesting polarization free of subsequent collision effects. We have thus measured the overall shape of each polarization spectrum at a rare-gas pressure of 20 Torr where the signals are relatively large. In order to determine how that shape changed as $P\rightarrow 0$, full pressure-dependent runs were then done at selected detunings.

Three-dimensional perspective graphs of all the Mg-Ne and Mg-Ar P_L data are presented in Figs. 7 and 8. These data are taken at a rare-gas pressure of 20 Torr in each case, and illustrate the general shape of the polarization surfaces as a function of Δ_1 and Δ_2. A global feature of the surfaces is a 100% polarization ridge occurring when $\Delta_1=-\Delta_2$; this corresponds to resonant excitation of the atomic Mg $3s\ ^1S_0\rightarrow 5s\ ^1S_0$ two-photon transition. Also seen is a general decrease of P_L as Δ_2 approaches zero, resulting in laser 2 probing of the polarization of the one-photon optical collision products in the Mg $3p\ ^1P_1$ level. In contrast, as $-\Delta_2$ is made larger than Δ_1, P_L remains significantly larger than on the other side of the two-photon atomic resonance. Generally, this range of detunings is associated with Mg–rare-gas collision pairs deeper in the molecular regime. Data taken with $\Delta_1=0$ and Δ_2 nonzero correspond to optical collisions between excited and aligned Mg $^1P_1$ atoms and RG atoms. Results for this excited-state optical collision process in Mg-Ar and Mg-Ne will be presented elsewhere.

To understand the detailed features of the complex P_L spectra, calculations on the fractional-collision process for these systems are required. However, all features may be tentatively understood by considering qualitative Mg-Ne and Mg-Ar molecular potentials for the transitions involved. Experimental potentials for the $3s\ ^1\Sigma_0^+$ and $3p\ ^1\pi_1$ electronic states in Mg-Ne and Mg-Ar have recently become available, and an estimate of the general location of the Mg-Ar $3p\ ^1\Sigma_0^+$ potential may be made from observed Λ doubling in $3p\ ^1\pi_1$ rovibrational levels [13]. Only calculated potentials for excited $ns\ ^1\Sigma_0^+$ molecular states in either Mg-Ar or Mg-Ne are available [15]. These show a generally quite strong binding of

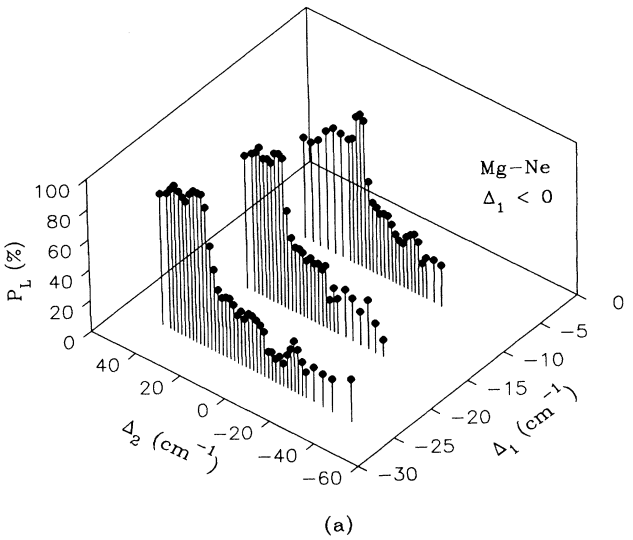

(a)

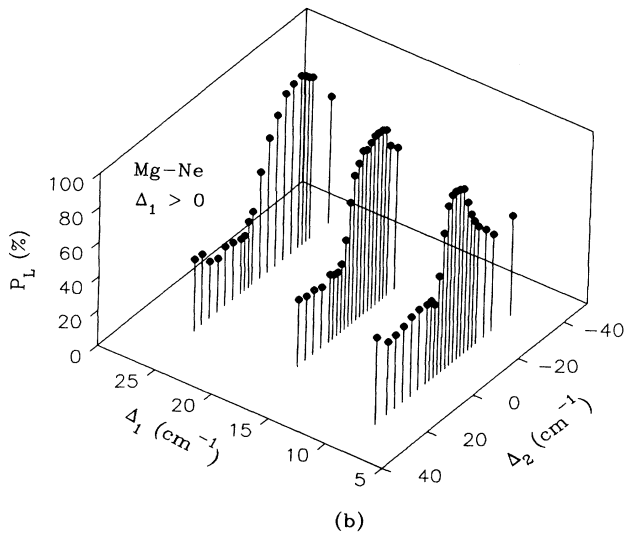

(b)

FIG. 7. Three-dimensional (3D) perspective of Mg-Ne fractional-collision polarization spectra for $P=20$ Torr. (a) $\Delta_1<0$. (b) $\Delta_1>0$.

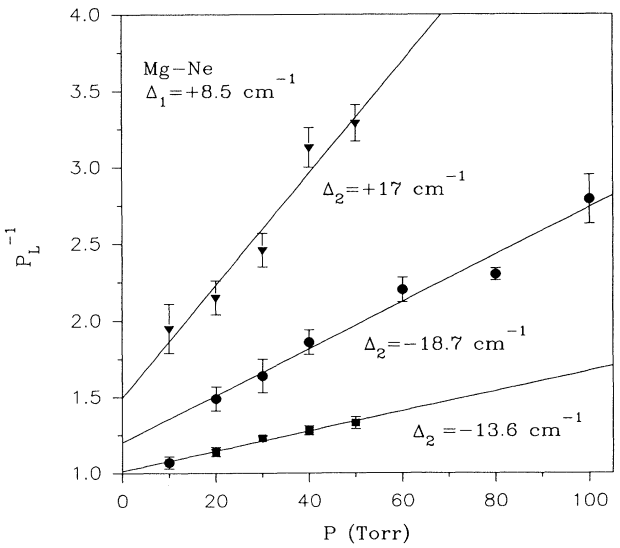

FIG. 6. Pressure dependence of Mg-Ne fractional-collision polarization when $\Delta_1=8.5$ cm^{-1} at several Δ_2.

several hundred cm^{-1} (with an equilibrium separation smaller than that of the $3p\ ^1\pi_1$ potential), and a repulsive barrier at long range ($R > 10a_0$). These features are consistent with results of measurements on excited $ns\ ^2\Sigma^+$ molecular states in Li-He and Li-Ne [24]. We consider only the largest detunings $\Delta_1 = \pm 25.5\ cm^{-1}$, for which a molecular picture is more likely to be qualitatively correct.

Discussion is based on the location of Condon points R_1 and R_2 for stepwise radiative transitions at the detunings Δ_1 and Δ_2. As delineated by vertical lines in Figs. 9 and 10 for nonzero detunings Δ_1, three ranges of Δ_2 must be considered. In any of these cases, rotation of the molecular alignment axis during the course of the optical collision leads to a reduction in the average polarization of the intermediate state. As the molecular electronic states investigated here are nominally singlets, additional depolarization due to spin-orbit interactions is expected to be negligible. A further important point is that, as the Mg-RG pair separates on an outgoing collision trajectory, the molecular alignment will eventually become decoupled from the body-fixed axis, and will become space fixed. This occurs within some range of R parametrized by a decoupling radius R_d [25]. When R_1 (R_2) $> R_d$, the measured P_L will vary weakly with Δ_1 (Δ_2). A general picture is then one in which an average molecular alignment is generated at some R_1, is dissipated on incoming and outgoing trajectories, and is probed at a second Condon point R_2. The available interatomic potentials allow approximate mapping of Condon points R to detunings Δ.

For $\Delta_1 = 25.5\ cm^{-1}$ in both Mg-Ar and Mg-Ne, the molecular potentials indicate that R_1 corresponds to excitation of the $3p\ ^1\Sigma_0^+$ dissociative state. For Mg-Ar, the

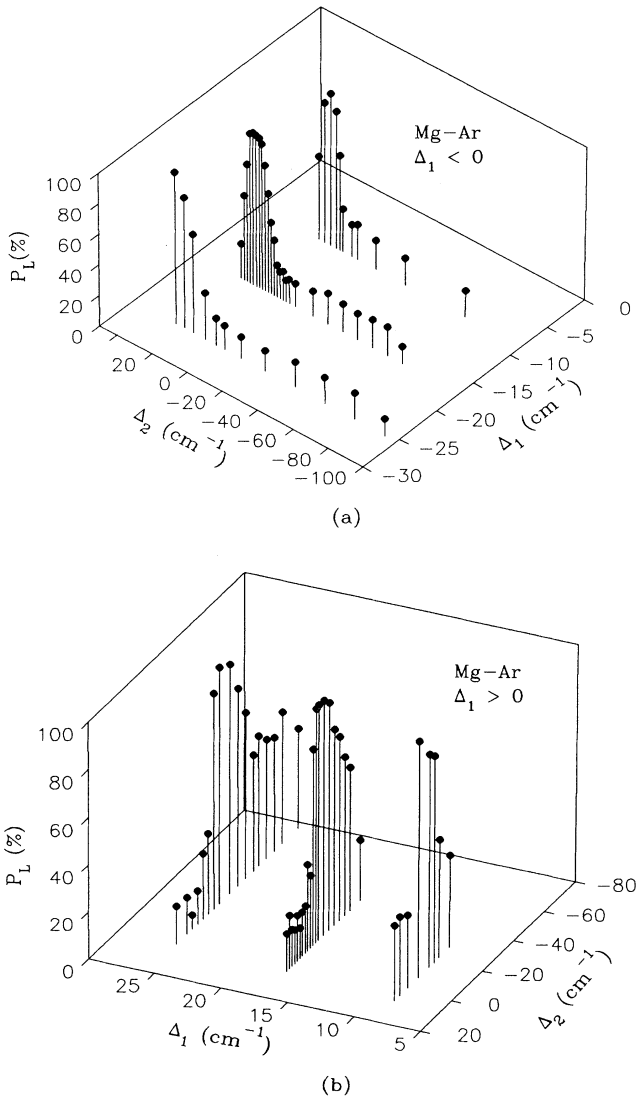

FIG. 8. 3D perspective of Mg-Ar fractional-collision polarization spectra for $P = 20$ Torr. (a) $\Delta_1 < 0$. (b) $\Delta_1 > 0$.

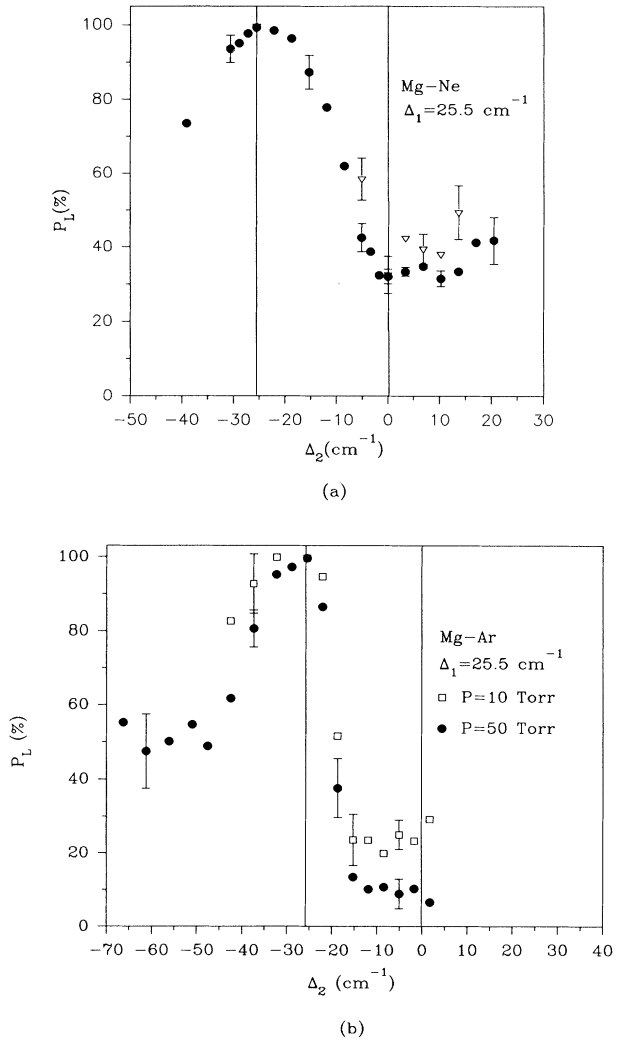

FIG. 9. Mg–rare-gas fractional-collision polarization spectra for $\Delta_1 = 25.5\ cm^{-1}$: (a) Mg-Ne, where 20-Torr spectra are indicated by solid circular data points. Low-pressure-limit extrapolations are shown as open triangles. (b) Mg-Ar.

potentials imply the possibility of two Condon points leading to excitation of the $3p\ ^1\Sigma_0^+$ state. Nevertheless, as seen in Fig. 9, the polarization spectra are qualitatively the same for each molecule, with P_L being largest when $-\Delta_2 > \Delta_1$, and having significantly smaller values when $-\Delta_2 < \Delta_1$. As $\Delta_2 \rightarrow 0$, P_L approaches a roughly constant value corresponding to the one-photon optical collision limit. The asymptotic value of P_L is approached as the Mg-RG separation nears R_d, where the molecular alignment is no longer coupled to the rotating molecular axis. The larger value of asymptotic polarization measured for Mg-Ne relative to that for Mg-Ar is expected on the grounds of the smaller reduced mass and more repulsive $3p\ ^1\Sigma_0^+$ potential for Mg-Ne; each situation leads to a greater rotational depolarization for Mg-Ar during the collision. When $\Delta_2 > 0$, optical excitation is, for the potentials considered here, mainly at long range where $R_2 > R_d$. Then the polarization remains approximately at its $\Delta_2 \rightarrow 0$ value. As $\Delta_2 \rightarrow -\Delta_1$, P_L rises, corresponding to less rotation of the molecular axis prior to probing at R_2. The existing potentials predict that there should be a confluence of the Condon points R_1 and R_2 when $\Delta_2 < 0$. Unfortunately, this apparently occurs also in the range where $\Delta_1 = -\Delta_2$, and where the spectrum is dominated by direct two-photon atomic absorption (see Figs. 4 and 5). Nevertheless, generally larger values of P_L are found in this spectral region. When $-\Delta_2 > \Delta_1$, the polarization also remains large, but again gradually decreases due to rotation of the molecular axis. As indicated previously, a possible second Condon point exists in Mg-Ne at smaller values of R_1 than probed in this experiment. There is no evidence of it in the polarization spectrum, where the polarization would be expected to rise as $R_2 \rightarrow R_1$.

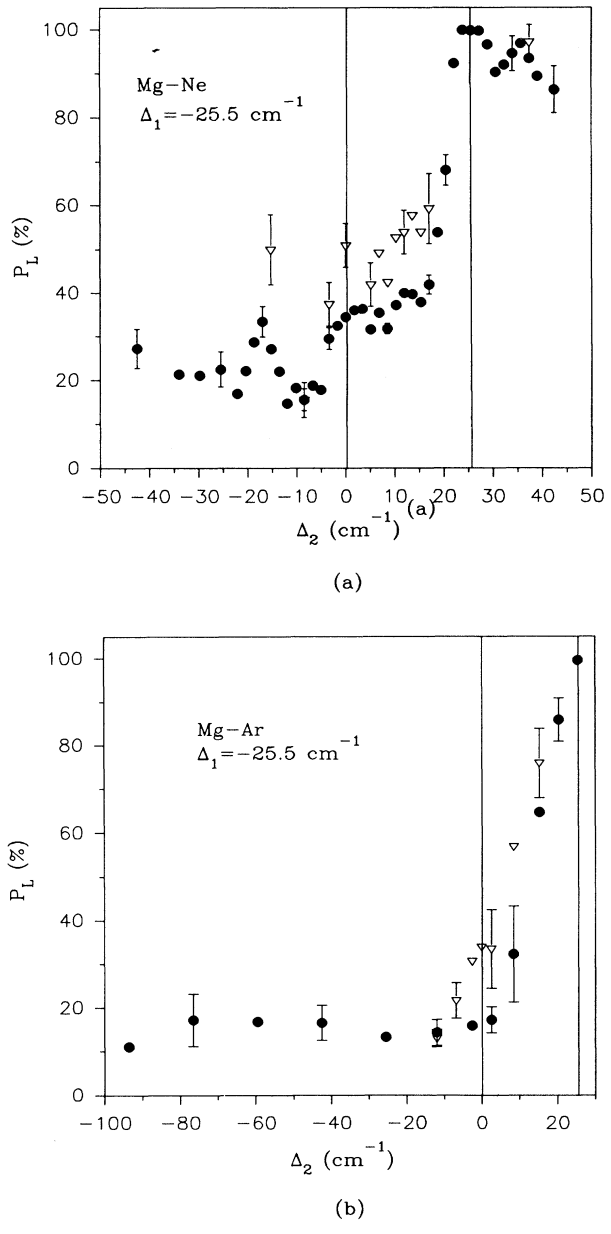

FIG. 10. Mg–rare-gas fractional-collision polarization spectra for $\Delta_1 = -25.5$ cm^{-1}. $P = 20$ Torr spectra are indicated by solid circular data points. Low-pressure-limit extrapolations are shown as open triangles. (a) Mg-Ne; (b) Mg-Ar.

When $\Delta_1 = -25.5$ cm^{-1}, excitation of the $3p\ ^1\pi_1$ occurs in both Mg-Ne and Mg-Ar. Existing potentials for Mg-Ar indicate that a second Condon point may also produce excitation of the $3p\ ^1\Sigma_0^+$. The polarization spectra given in Fig. 10 show qualitative similarities for the two molecules. However, for Mg-Ne the polarization spectra show the pressure dependence described in the previous paragraphs while the fractional-collision signal rise increases linearly with the intensity of each laser. These features are characteristic of a free-free fractional-collision signal. On the other hand, when $\Delta_2 < 0$ for Mg-Ar the polarization spectra are weakly dependent on Ar pressure (for Ar pressure < 50 Torr) and the excitation spectra show saturation with the intensity of laser 2. This behavior may be explained as due to bound state excitation in the intermediate $3p\ ^1\pi_1$ potential. For that case, the excitation spectra can show saturation due to a high density of unresolved rovibrational transitions. The measured P_L can also be quite immune to collisional reduction, for the average angular momentum of the typical rovibrational level in the $3p\ ^1\pi_1$ would be large, while the radiative lifetime of the $3p\ ^1\pi_1$ electronic state is short (~ 2 ns). Under these conditions, the measured polarization for broadband excitation should be in the 20–30 % range, depending on the relative density of P-, Q-, and R-branch transitions in the spectral region excited by laser 1 and probed by laser 2 [12].

The Mg-Ne P_L spectra when $\Delta_1 = -25.5$ cm^{-1} show a variety of interesting features. First, when $\Delta_2 > -\Delta_1$, the $3p\ ^1\pi_1$ amplitude generated by laser 1 is probed by two Condon points arising from the barrier in the $5s\ ^1\Sigma_0^+$ potential (see Fig. 1). These points correspond to probing the amplitude near the point of excitation R_1, implying a large polarization as seen in Fig. 10. In the spectral region where $-\Delta_1 > \Delta_2 > 0$, one of the Condon points migrates to long range where it should dominate the probing signal, while the other remains at shorter range and

in the vicinity of R_1. As evident in Fig. 10, the polarization does asymptotically go to a lower and nearly constant value when $\Delta_2=0$ (the one-photon optical collision result in an impact limit). In the third region, where $\Delta_2<0$, the longer-range Condon point becomes antistatic, and the probe signal dominated by the short-range amplitude in the $3p\ ^1\pi_1$ state. It would appear from the data in Fig. 10 that this happens abruptly around $\Delta_2=-5\ \text{cm}^{-1}$, where P_L exhibits a sharp decrease. This is followed by a narrow region of increased polarization around $\Delta_2=-18\ \text{cm}^{-1}$; the localized area of increase is very reproducible. The origin of this complex behavior is not clear, but may be due to a combination of bound level and free-free scattering contributions to the spectra. A recent spectroscopic study [14] of Mg-Ne showed that the 0-0 band of the $3s\ ^1\Sigma_0^+ \rightarrow 3p\ ^1\pi_1$ electronic transition has a band head near $\Delta_1=-25\ \text{cm}^{-1}$, nearly coincident with the detuning corresponding to the data in Fig. 10. An associated intensity structure which would implicate bound-bound transitions to the $5s\ ^1\Sigma_0^+$ potential is not evident in Fig. 5(b). However, for Mg-Ne it is expected that the mean thermal energy is much larger than the average rotational energy, and that any rovibrational bands in the intensity spectra would be spectrally broad. We point out that a band head in one branch of a rovibrational band may show up more clearly in a polarization spectrum than in an intensity one. This occurs because a polarization spectrum is constructed so as to display differences in intensity, rather than the overall spectral shape of the strength of a process.

V. CONCLUSIONS

In conclusion, fractional-collision studies represent a promising way to learn about atomic collision dynamics and about the interaction of electromagnetic radiation with colliding atoms.

A combination of pressure-dependent polarization and excitation spectra is necessary to extract the largest amount of information about the physical system, including that from spectral regions dominated by transitions between bound levels or representing continuum scattering of the particles and radiation. The spectra are rich in structure as a function of detuning and polarization of both the pump and the probe lasers. For Mg-RG spectra, multiple Condon point effects may also be important to interpretation of the results. However, it is evident that detailed calculations for these systems will be necessary in order to extract dynamical information about the data, and to assess the relative importance of direct and stepwise two-photon contributions to the fractional-collision spectra. Elaborations of simpler approches such as the Lewis-Cooper [25] model would be very helpful in guiding qualitative discussions of the spectral excitation and polarization features.

ACKNOWLEDGMEMTS

The financial support of the National Science Foundation (Grant No. PHY-9121957) is greatly appreciated. One of us (R.A.L.) acknowledges the support of the Patricia Roberts Harris Fund.

*Present address: Physics Department, Lynchburg College, Lynchburg, VA 24501.

†Permanent address: Physics Department, Central Michigan University, Mount Pleasant, MI 48859.

[1] *Atomic and Molecular Beam Methods,* edited by Giacinto Scoles (Oxford University Press, New York, 1988), Vol. 1.

[2] A. H. Zewail, Science **242**, 1645 (1988); L. R. Kundekar and A. H. Zewail, Annu. Rev. Phys. Chem. **41**, 15 (1990).

[3] K. Burnett, Phys. Rep. **118**, 339 (1985).

[4] W. Behmenburg, Phys. Scr. **36**, 300 (1987).

[5] D. A. Olsgaard, M. D. Havey, and A. Sieradzan, Phys. Rev. A **43**, 6117 (1991).

[6] S. J. Singer and K. F. Freed, J. Chem. Phys. **79**, 6060 (1983); V. Zafiropulos, P. D. Kleiber, K. M. Sando, X. Zeng, A. M. Lyyra, and W. C. Stwalley, Phys. Rev. Lett. **61**, 1485 (1988).

[7] R. A. Lasell, D. A. Olsgaard, and M. D. Havey (unpublished).

[8] D. A. Olsgaard, M. D. Havey, A. Sieradzan, and R. A. Lasell, Phys. Rev. Lett. **69**, 1745 (1992).

[9] G. Nienhuis and F. Schuller, Physica (The Hague) **94C**, 394 (1978).

[10] S. Yeh and P. R. Berman, Phys. Rev. A **22**, 1403 (1988).

[11] G. Alber and J. Cooper, Phys. Rev. A **31**, 3644 (1985).

[12] C. H. Greene and R. N. Zare, Annu. Rev. Phys. Chem. **33**, 119 (1982).

[13] R. R. Bennett, J. G. McCaffrey, I. Wallace, D. J. Funk, A. Kowalski, and W. H. Breckenridge, J. Chem. Phys. **90**, 2139 (1989).

[14] Ingvar Wallace and W. H. Breckenridge, J. Chem. Phys. **98**, 1 (1993).

[15] M. Hliwa and J. Daudey, Chem. Phys. Lett. **153**, 471 (1988); E. Czuchaj, F. Rebentrost, H. Stoll, and H. Preuss, *ibid.* **182**, 191 (1991).

[16] A. A. Radzig and B. M. Smirnov, *Reference Data on Atoms, Molecules, and Ions* (Springer-Verlag, Berlin, 1985).

[17] K. Blum, *Density Matrix Theory and Applications* (Plenum, New York, 1981).

[18] G. Herzberg, *Spectra of Diatomic Molecules,* 2nd ed. (Van Nostrand Reinhold, New York, 1950).

[19] W. Demtroder, *Laser Spectroscopy* (Springer-Verlag, Berlin, 1982).

[20] L. L. Vahala, P. S. Julienne, and M. D. Havey, Phys. Rev. A **34**, 1856 (1986).

[21] F. A. Jenkins and H. E. White, *Fundamentals of Physical Optics* (McGraw-Hill, New York, 1937).

[22] M. Belsley, W. J. Alford, K. Burnett, and J. Cooper, J. Quant. Spectrosc. Radiat. Transfer **35**, 53 (1986).

[23] Dieter Zimmerman, Trends Chem. Phys. **1**, 391 (1991).

[24] C. J. Lee and M. D. Havey, Phys. Rev. A **43**, 6066 (1991).

[25] E. L. Lewis, M. Harris, W. J. Alford, J. Cooper, and K. Burnett, J. Phys. B **16**, 553 (1983).